SIDE VENTING VERSUS END VENTING FOR LARGE L/D VESSEL EXPLOSIONS WITH AND WITHOUT AN OBSTACLE

A. Alexiou, G. E. Andrews, H. Phylaktou and C. L. Gardner
Department of Fuel and Energy Leeds University Leeds LS2 9JT

The influence of side venting on explosions in a large length to diameter ratio (L/D=13.9) vessel with and without an obstacle was evaluated and compared to end vented explosions. A number of pressure peaks were measured, due to different stages of the explosion. During side vented explosions without an obstacle it was found that the pressure oscillations in the combustion of the trapped unburnt gas was the dominant phase of the explosion. During end-vented explosions the dominant event was the external explosion. With the obstacle in place the external explosion dominated the explosion development for both the side and end vented tests. The maximum overpressure for side venting with an obstacle was higher than for end venting due to rapid combustion of the trapped end gases.
Keywords: Explosions, Venting, Overpressures.

INTRODUCTION

Relief vents are widely used in industry to protect industrial installations from internal explosions. Unburnt mixture and combustion products are discharged to the atmosphere, thereby restricting the explosion pressure to a value not exceeding the mechanical strength of the vessel. Although the current design guidelines for large length to diameter ratio (L/D) vessels such as NFPA 68 (1) are based on few experimental investigations, side-venting is particularly recommended to protect pipe lines and ducts. Recently, systematic work on side vented explosions in large L/D vessels by the authors confirmed that the closer the side-vent was to the ignition source the lower was the overpressure achieved, but this overpressure was always higher than the overpressure for end venting (2). It has been shown that in many cases irrespective of the number of side vents and of the vent position the maximum overpressure achieved was above 0.4 bar (3). This was due to the unburnt gas mixture trapped between the last side vent and the end-flange of the vessel which burnt with strong oscillatory pressure waves and produced a higher overpressure. It was concluded that side venting should only be used in conjunction with an end vent as in the original work of Rasbash and Rogowski (4).

Obstacles in the path of a propagating flame interact with the explosion-induced flow to generate turbulence which in turn accelerates the flame resulting in a more severe explosion. Obstacles have an aggravating effect on an explosion; they make an explosion risk situation potentially more damaging and result in more stringent safety requirements. In the design of vents for explosions, the creation of turbulence due to an obstacle ahead of the flame results in a larger vent area requirement than for an empty vessel for the same overpressure. The increase in the vent area is directly proportional to the increase in the mass burning velocity of the flame due to the effect of the obstacle. Alexiou et al. (5) studied the effect of obstacles in end vented explosions and found that the overpressure increased by a factor of up to 11 with an increase in blockage ratio (BR) to 60%. This was due to the increase in turbulence created by the obstacle in the unburnt gas ahead of the flame front. Rasbash and Rogowski (4) reported similar results for end vented explosions. They also found a reduction in overpressure by

inserting a relief vent near the ignition source in addition to the end vent. The reduction in overpressure was dependent on the size of the additional vent.

In this work we compare end vented tests with side vented tests (single vent) in a large L/D vessel with and without an obstacle of BR=40%. The objective was to look the fundamental phenomena characterising the explosion and quantifying the influences that lead to the observed overpressures.

EXPERIMENTAL TECHNIQUES

The side vented explosions were carried out in a horizontal cylindrical vessel 0.154-m in diameter with an L/D of 13.9. The vessel was constructed with four side vents (four 90° T-junctions) of 0.154-m diameter. This rig was originally constructed to investigate the influence of multiple side venting on explosion development and it is different from the rig used in previous reported work (2). The four side legs were always present in the present set-up whether they were utilised as vents or not. Burning pockets of gas left in these legs after the passage of the main flame could have affected the explosion development. However, there is no evidence of a major influence there. The first vent centreline distance from the end-flange was 0.25-m and the others were spaced at 0.5-m apart as shown in Figure 1a. The explosion was vented into a 0.5-m-diameter 2-m-long vessel with three side vent mounting flanges on 0.5-m centreline spacing. This was connected by a pipe, 0.162-m-diameter 1.5-m-long, to another vessel of 0.5-m-diameter 1-m-long. These two vessels were used as a dump volume to allow vented experiments to be carried out safely in the laboratory. The test to dump volume ratio was approximately 1/15. The end vented explosions were carried out in a cylindrical vessel 0.162-m in diameter with an L/D ratio of 15.4, shown schematically in Figure 1b. The same dump volume was used to vent the explosion overpressure.

The vent was fully open throughout this work with a vent area equal to the vessel cross sectional area. In the side vented explosions the vent was placed at 9.1D from the spark whereas in end vented explosions the vent was at the end of the vessel (15.4D from the spark). The obstacle was a single hole orifice plate of 40% blockage ratio, placed at 4.0D from the spark. For the end vented explosions the obstacle was located at 6.2D from the spark. A vacuum gate valve was used to separate the test section from the dump vessel which was filled with air. The initial pressure in both sections (test section and dump section) was 1 atm and the gate valve was opened just prior to ignition, thus any movement of gas or air from one section to another was restricted. The one atmosphere gas/air mixture in the test vessel was formed by partial pressures and a homogeneous composition was achieved by circulating the mixture in the explosion vessel using an external recirculating pump. The mixture was then ignited with a spark, flush with the end-flange of the explosion vessel. The flame travel was recorded by a centreline axial array of mineral insulated, exposed junction, type K thermocouples. Thermocouples were also placed along the axial centreline of the vent and in the dump vessel. The time of flame arrival was detected as a sharp change in the gradient of the voltage output of the thermocouple and in this way the average flame speed between any two thermocouples could be calculated. The pressure variation was recorded using a series of KELLER pressure transducers (Pa, Pb, Pc) mounted at different places in both the explosion and dump vessel as shown in Figure 1.

In order to eliminate the small pressure rise in the total closed volume due to the dump vessel effect, the overpressures reported here were taken by subtracting the pressure recorded by the pressure transducer in the dump vessel from the pressure recorded by the pressure transducer in the test section. This technique was validated by undertaking free end vented explosions in the laboratory using a 76 mm diameter pipe. This pipe size allowed safe vented explosions in the laboratory. The results showed that the free vented explosion had the same maximum overpressure (relative to the atmosphere) with the

explosion vented into the dump vessels (relative to the dump vessel). Also the same stages of the explosion event were recorded.

A fast (200 kHz per channel) 34 channel transient data acquisition system was used to record the thermocouple and pressure transducer data. A mixture of 10% methane in air was used in all tests. Each test was repeated at least three times and averaged readings for the peak overpressure are reported here. Typical test to test variations in the peak overpressure for the same test geometry was 5% of the peak pressure.

PRESSURE TIME RECORDS

During end vented explosions without an obstacle, Alexiou et al. (6) identified three pressures peaks based on three different phases of the explosion development as shown in Figure 2. The first pressure peak (P1) was due to an elongated "U" flame observed in large L/D vessels, where the flame accelerates in the axial direction and is associated with higher combustion rate due to a large flame surface area. Once the "skirt" of the elongated flame reached the tube wall the rate of production of burnt gas decreased due to a reduction in flame area and the internal pressure started to fall. The turbulence of the unburnt gas flow induced by the initial fast flame, in the downstream pipe, resulted in flame reacceleration due to turbulent combustion and this gave rise to a second pressure peak (P2). When the flame reached the vent, the mixture of unburnt gas previously vented was ignited and a third pressure peak, P3, due to the external explosion was observed and this was the peak overpressure. In the presence of an obstacle the same three pressure peaks were identified as shown in Figure 3. However, the magnitude of the pressure peak P2 was much higher compared to that without an obstacle and this was due to the increase in turbulence created by the obstacle.

Typical pressure-time histories for side vented explosions without an obstacle and with an obstacle of 40% blockage are shown in Figures 4 and 5 respectively. These figures are based on the pressure difference between the pressure transducers Pb and Pc, as discussed previously. On these figures the times that the flame reached the obstacle, the vent and the far end-flange, ($t_{obst.}$, t_{out}, t_{end}) are also marked.

In side vented explosions without an obstacle (Figure 4) three pressure peaks were identified; P1 and P3 due to the initial phase and to the external explosion, respectively and P4 due to the oscillations set up in the system as the trapped gas burnt. The peak oscillatory pressure was associated with the flame arrival at the end-flange. The pressure peaks P1 and P3 were due to the same events as in the end vented explosion. The pressure peak P4 was due to the combustion of the trapped unburnt gas mixture between the side vent and the end of the vessel and is a characteristic of side vented explosions. This trapped unburnt gas, which has to exit as burnt gas through the side vent, is the key difference from the end vented explosions. Figure 4 shows that the flame propagation from the side vent position to the far end-flange was slow as indicated by the time of flame arrival at the far end-flange. The overpressure due to the pressure oscillations (P4) took place at the far end-flange and was found to be the dominant phase of the explosion. The pressure peak due to the turbulence (P2) was not observed because there was insufficient distance for the flame to accelerate into the turbulent phase that gave rise to P2 in the end vented explosions. Comparing Figures 4 and 5 it can be seen that there is a difference between the phenomena which control the magnitude of the overpressure. Whereas without the obstacle the controlling phase was due to the pressure oscillations set up in the system, with the obstacle in place the controlling phase was due to the fast turbulent flame downstream of the obstacle. This created a high velocity jet out of the side vent and an increase in the external explosion (P3).

Figure 6 shows the same pressure-time record as Figure 5, but it concentrates on the portion

where flame propagation in the enhanced turbulence due to the obstacle is taking place, which is immediately downstream of the obstacle near the vent. In Figure 6 four pressure peaks were identified; P1 due to the initial "U" flame shape, P2 due to the enhanced turbulence created by the obstacle, P3 due to the external explosion downstream of the vent and P4 due to the pressure oscillations in the trapped unburnt gases as they burnt. The significant increase in overpressure P3 was due to the increase in turbulence by both the obstacle and the flow out of the side vent. Figure 7 shows the same pressure-time history as Figure 6, but using the pressure difference between the pressure transducers Pa and Pc. It is clear that although the same phases of the explosion were observed the absolute value of the maximum overpressure was much lower compared to Figure 6. This was due to the pressure losses across the obstacle as shown directly by (Pa-Pb) in Figure 8. This shows that initially Pa>Pb as the initial explosion expansion pushed unburnt gas through the obstacle. The accelerated combustion downstream of the obstacle resulted in a very high unburnt gas flow rate out of the side vent, producing the peak (Pa-Pb) pressure difference of 0.4 bar just prior to the flame exiting the vent. The violent external explosion which then occurred caused a large pressure rise P3 inside the vessel which compressed the burnt gases and forced a reverse flow of burnt gas back across the obstacle at a very high rate with a large pressure difference of 1 bar, indicating a pressure ratio of 2 and sonic flow conditions at the obstacle. The peak overpressures which were measured and given below for side vented explosions were based on the pressure difference between Pb and Pc as the volume between the obstacle and the far end of the vessel experienced the highest overpressures.

PEAK OVERPRESSURES

As mentioned above four different pressure peaks were observed in the side vented tests due to different events taking place. These pressure peaks were measured and are shown in Table 1.

Table 1. Overpressures measured during the different stages of the explosion.

Overpressures	Based on Pb-Pc		Based on Pa-Pc	
	Side Venting BR=0%	Side Venting BR=40%	End Venting BR=0%	End Venting BR=40%
P1 (Initial Phase)	59	26	71	103
P2 (Turbulent Phase)	-	756	62	701
P3 (External Explosion)	589	1658	547	785
P4 (Oscillatory Phase)	766	1244	-	-

Also shown on this table are the overpressures for the end vented explosions. The reported overpressures for end venting are based on the pressure difference between Pa and Pc, since the highest overpressures were obtained this way. As was discussed above, during side vented explosions without an obstacle the maximum overpressure was due to the pressure oscillations (P4) set up in the trapped unburnt gas mixture between the side vent and the end-flange. This overpressure reached a maximum value of 766 mbar, higher than the maximum overpressure during the equivalent end vented explosion (547 mbar). The maximum overpressure during end vented explosions was due to the external explosion (P3) which was almost of the same magnitude as the external explosion for side vented explosions without an obstacle. During side-vented explosions with an obstacle of BR=40% the maximum overpressure was due to the external explosion (P3). This was due to the vent jet turbulence which was enhanced by the presence of the obstacle and the side vent. This overpressure was much higher than the maximum overpressure for end vented explosions (which was due to the external explosion, P3). The overpressure due to the turbulent phase (P2) prior to the flame exiting the vent, was almost of the same

level for both configurations indicating that similar turbulent levels were present downstream of the obstacle. In end vented explosions the overpressure P1 (due to the initial phase of the explosion) was observed to be higher than for side vented explosions. This was because in the end vented explosions the obstacle was placed further downstream the tube at 6.2D compared to 4.0D for side venting, which resulted in a more established elongated initial flame acceleration and a faster flame upstream of the obstacle.

FLAME SPEEDS

A comparison of the flame speeds with and without an obstacle of 40% blockage is shown in Figure 9 for side vented explosions where the flame speed is plotted as a function of the dimensionless ratio X/D. On this figure are also shown the positions of the obstacle as well as the vent. Without an obstacle the flame speed continues to accelerate until it reached the side vent where it then decelerated in the trapped gas region The flame speed approaching the end-flange was 6.8 m/s and effectively was the burning velocity as the flame expansion was in the burnt gas region out of the vent. With an obstacle of BR=40% in place the flame speeds is much higher than without the obstacle. This was due to the turbulence created by the obstacle as well as by the side vent. The flow around the vent splits into two; one carries further downstream the tube towards the end-flange and one out of the vent and into the dump vessel. Compared to end vented explosions without an obstacle the maximum flame speed was in the order of 120m/s, higher than for the side vented explosion, as shown in Figure 10. This was due to the fact that with end vented explosions there was nothing to stop the acceleration of the unburnt gas flow, ahead of the flame front, and it continue to accelerate until the end of the tube. With an obstacle of BR=40% in place the maximum flame speed was in the order of 820m/s, much higher than for the side vented explosion. This was again due to the same reason as without an obstacle, as well as the obstacle being further downstream the tube at 6.2D (compared to 4.0D with side venting).Therefore, there was a much higher initial flame acceleration approaching the obstacle and hence a higher flame speed downstream of the obstacle and induced gas flow towards the open end of the tube.

ESTIMATED TURBULENT COMBUSTION PARAMETERS

It is evident from the previous discussion that the critical explosion phase in these tests was the propagation of the flame upstream of the vent and the external explosion. In this section an attempt will be made to estimate the turbulence levels and the turbulent combustion parameters that were induced upstream of the vent and in the external explosion and in the stages before the flame reached the vent. This analysis will support the above qualitative explanation of the observed overpressures. The external explosion is characterised by the turbulence induced by the unburnt gas jet discharged from the pipe into the dump chamber.

Basic Equations

The unburnt gas vent discharge velocity is controlled by the flame speed upstream of the vent, which is directly influenced by the obstacle. The influence of the obstacle is also determined both by its blockage and the upstream flame speed, which determines the unburnt gas velocity across the obstacle. The combustion is described by the turbulent burning velocity S_T. Phylaktou and Andrews (7) reported a turbulent combustion correlation based on explosion data, which for methane reduces to:

$$\frac{S_T}{S_L} = 1 + 0.67 \left[\frac{u'}{S_L}\right]^{0.47} R_\ell^{0.31} \qquad (1)$$

where S_L is the laminar burning velocity, u' is the root mean square of the fluctuating velocity of the turbulent flow field and R_ℓ is the turbulent Reynolds number given by:

$$R_\ell = \frac{u'\ell}{\nu} \tag{2}$$

where ℓ is the integral length scale of turbulence. For a constant length scale or similar variation in ℓ, Phylaktou et al (8) have shown that most hydrocarbon-air turbulent burning velocity data fit the empirical expression:

$$\frac{S_T}{S_L} = 1 + 2\frac{u'}{S_L} \tag{3}$$

Equation 3 is useful when the variables in equation (1) are not all known.
Phylaktou and Andrews (9) showed that the turbulence levels in a flowing system are related to the pressure losses according to:

$$u'/S_g = C_T\sqrt{K} \tag{4}$$

where S_g is the mean flow velocity C_T is a proportionality constant (less than 0.58, which is the theoretical value for complete conversion of the pressure energy loss to turbulent energy) and K is the pressure loss coefficient given by:

$$K = \frac{\Delta P}{\frac{1}{2}\rho S_g^{\,2}} \tag{5}$$

where ΔP is the pressure difference and ρ is the density of the unburnt gas. The pressure loss coefficient is characteristic of the flow geometry and fairly independent of the flow velocity. Values of K for different flow geometries are reported in several studies in the literature some of which will be referenced below.

An alternative to equation (4) for steady state fully developed turbulent flows in pipes is given by the empirical correlations of Abdel-Gayed and Bradley (10);

$$\frac{u'}{S_g} = 0.168\,Re^{-0.119} \tag{6}$$

and

$$R_\ell = 13.45\times10^{-3}\,Re^{0.902} \tag{7}$$

where Re is the pipe Reynolds number ($Re=S_gD/\nu$, with D the pipe diameter and ν the kinematic viscosity).

The flame speed (S_f) in any explosion is related to the burning velocity and the S_g by:

$$S_f = ES_T$$

$$S_g = S_f - S_T = S_T(E-1) = Sf\left[1 - \frac{1}{E}\right] = 0.87S_f \quad (8)$$

where E is the expansion ratio (equal to 7.49) for an adiabatic explosion but smaller if there are heat losses, as in the present work. For an adiabatic explosion $S_g = 0.87\ S_f$ but Phylaktou and Andrews (11) showed that for explosions in pipe configurations $S_g = 0.8\ S_f$ because of the heat losses. This equation will be used to estimate S_g from the measured S_f and also to estimate S_f from the predicted S_g.

External Explosion

For both the end and side vented configurations the dump vessel discharge corresponds to an internal flow undergoing a sudden expansion from a pipe outlet for which the typical pressure loss coefficient (K) for air at low velocities and with an area ratio of about 0.1 is 0.8 (12). For side venting the flow undergoes a division at the vent "T" piece junction with the majority of the flow going through the "T" branch. The pressure loss coefficient in this case is equal to K=1.1 (13). Therefore, for the side vented tests the flow goes through two major changes before the external explosion occurs. A direction change through the vent "T" piece followed by an enlargement into the dump. The total pressure loss coefficient will be the accumulative effect for the two changes (K=1.1+0.8=1.9) for incompressible flow. The total pressure loss (ΔP) of the flow in the present tests was measured as the pressure difference between the pressure transducers Pb and Pc (see Figure 1) at the time of the flame arrival at the vent. These measurements and the pressure loss coefficient equation (5) were used to estimate the induced unburnt gas velocity through the vent. The values of K, measured pressure loss ΔP and the calculated gas velocity, S_{g2}, are shown in Table 2. It should be noted that the gas density, ρ, was corrected for the absolute system pressure (shown as Pb) at the time t_{out}, assuming isentropic compression of the unburnt mixture. Furthermore, the values of K on this table were corrected for the appropriate mach number, which increased to above the incompressible flow value (12,13).

Having estimated the unburnt gas velocities at appropriate values of K equation (4) was used to estimate the rms turbulent velocity u'. The proportionality constant C_T was taken to be 0.076 which is the appropriate value for a thick orifice or nozzle (9).It was now possible to estimate the turbulent to laminar burning velocity ratio (S_T/S_L) in the vent discharge using equation (3). Equation (3) was used instead of equation (1) because of the difficulty in assigning an appropriate length scale, ℓ, to the discharge flow. The calculated values of u' and S_T/S_L for the vent discharge flow just prior to the external explosion are shown in Table 2 for the different test configurations. It can be seen that the turbulent combustion parameters for the side vent are similar with those for the end vent for both conditions studied here (with and without an obstacle). On this basis it would be expected that the corresponding overpressures due to the external explosion should be of a similar magnitude. The measured overpressure for the peak P3 in Table 1 do not support this, but as explained before the values shown are based on the transducers that gave the maximum overall overpressures which were different for side venting as compared to end venting. However, based on the pressure transducers difference between Pa and Pc, Table 2 shows that the external explosion was of similar magnitude for both the side and the end venting, for the two condition studied (with and without an obstacle). This was in agreement with the predicted turbulent combustion characteristics as shown. The above calculations were based on the pressure loss measurements between the test and the dump vessels just before the external explosion events which are mainly influenced by the presence of the obstacle. The use of Pa-Pc to determine the vent exit velocity is not ideal and a pressure transducer by the vent would be preferable. The use of Pa includes the obstacle pressure loss, if there is any remaining expansion behind the obstacle when the

flame exited the vent. Also it includes flow friction pressure losses upstream of the vent. For these reasons an estimation of the vent upstream flow was undertaken based on the flow induced across the obstacle.

Table 2. Turbulent flow and turbulent combustion characteristics in the vent discharge flow at the time just prior to the external explosion.

BR (%)	ΔP (bar)	K	Pb (abs) (bar)	T (K)	ρ kg/m^3	S_{g2} (m/s)	u'	S_T/S_L	P3 (Pa-Pc) (bar)
0 (Side vent)	0.109	2.0	1.147	307	1.3	91	9.8	44.7	0.563
40 (Side vent)	0.738	2.1	1.795	349	1.79	189	21.8	97.9	0.751
0 (End vent)	0.060	0.8	1.217	312	1.36	105	7.2	32.8	0.547
40 (End vent)	0.701	1.0	1.840	351	1.83	277	21.1	94.6	0.785

Obstacle Induced Turbulence and Turbulent Combustion

The plot of ΔP=Pa-Pb in Figure 8 shows that in the early stages of the explosion there was a static pressure difference across the obstacle due to the flow induced across the obstacle. The position of the pressure transducers (Pa and Pb) did not only measure the pressure loss due to the obstacle but it also included friction losses along the length of the pipe and additional losses due to the dividing flow at the vent plus losses at the three blocked off tee-branches along the pipe. The pressure loss coefficient due to the obstacle was calculated as being 1.8 (9), while dividing flow at the vent gives a pressure loss coefficient along the rim of the tee of 0.35 while each of the blocked tee-branches contributed a K of 0.05. Considering that there is approximately one frictional dynamic head loss (K=1) for every 60D of pipe then the frictional pressure loss of the present vessel was K=0.23. Adding all of the above gives an overall pressure loss coefficient between the two pressure transducers of K=2.53 (13). This was used in equation (5) in conjunction with the pressure difference (ΔP=Pa-Pb) just prior to the flame arrival at the obstacle to calculate the unburnt gas velocity S_{g1} as shown in Table 3. Also shown in Table 3 are the measured flame speeds S_{f1} upstream of the obstacle. The computed gas velocities, S_{g1}, should have been smaller (≈ 80%) of the flame speeds, instead of comparable values as shown in Table 3. This was probably due to the relative poor spatial resolution of the flame speed (≈ 0.13 m) as compared to continuous temporal resolution of the gas velocity through the pressure record. Thus the peak flame speed could have been higher than that measured, but existing only for a short distance.

Table 3. Induced gas velocities through the obstacle and turbulent combustion parameters downstream the obstacle.

BR=40%	ΔP (mbar)	S_{g1} (m/s)	R_f	u'	S_T/S_L	S_{f2} (m/s)	S_{g2} (m/s)	S_{f1} (m/s)
Side vent	36	48	18996	14.5	74	248	198	43
End vent	90	77	30472	23.2	106	357	286	80

Based on equations 4, 2 and 1 and using C_T=0.225 (9) the turbulent combustion parameters downstream of the obstacle were calculated. All the computed parameters are shown in Table 3. The calculated flame speeds, S_{f2}, and the unburnt gas velocities downstream of the obstacle were obtained from equation (8). Comparison of S_{g2} predicted in Table 3 with those determined from Pa-Pc at the time the flame exits the vent, in Table 2, show higher values. This indicates that the use of pressure transducer Pa may have underestimated the vent exit velocity and hence the severity of the external explosion in Table 2. However, the difference could have been due to the heat losses and a lower value of E in

equation (8). Considering the uncertainties in both methods the agreement on the value of S_{g2} is reasonable.

Pipe Flow Turbulence Downstream of the Obstacle

From the estimated flame speeds downstream of the obstacle (shown in Table 3) the induced unburnt gas flow could be estimated, which is approximately 80% of the flame speed. (10) Having estimated the unburnt gas flow the turbulent parameters could be calculated based on the equations 1, 6 and 7. The flame speeds, S_{f3}, were calculated based on the following equation:

$$S_{f3} = (S_T E) + S_g \qquad (9)$$

This equation assumes a two stage combustion process whereby the explosion upstream of the obstacle induces a flow with turbulence downstream of the obstacle. However, once the flame reaches the obstacle there is no further flow across the obstacle and a plug flow of unburnt gas moves at S_g down the tube. The flame burning this mixture expands the gas and this is all channelled in the direction of the vent, increasing the unburnt gas velocity ahead of the turbulent flame.

These turbulent parameters are shown in Table 4 and it can be seen that the estimated flame speed (S_{f3}) for end vented explosions, further downstream in the vessel, is in very good comparison with the measured flame speed ($S_{f3\ meas.}$). However, the equivalent measured flame speed for side vented explosion is much lower than the calculated flame speed. This was probably due to vent position being closer to the obstacle and hence there was no third stage flame acceleration prior to the vent.

Table 4. Induced gas velocities and turbulent combustion parameters further downstream the pipe.

BR=40%	S_{g2} (m/s)	R_f	u'	S_T/S_L	S_{f3} (m/s)	$S_{f3meas.}$ (m/s)
Side vent	198	669577	3.2	109	566	225
End vent	286	632683	4.7	127	715	860

The predictions in Table 2 and Table 3 all show that the severity of the external explosion, in terms of the unburnt jet velocity and subsequent turbulent jet flame speed, with side venting was less than with end venting. This makes it difficult to explain why P3 in Figure 6 (for Pb) was higher than P3 or P2 in Figure 3 for end venting with an obstacle. Comparison with Pb for end venting shows that the difference was not due to the transducer position. Consequently, it must be concluded that the large P3 in Figure 6 was associated with the trapped end gas combustion, but was not due to pressure wave effects, as Figure 5 shows them to be set up after P3 and at a lower magnitude. It is considered that the effect is due to the fast flame at 200 m/s in Figure 9 "overshooting" the vent location giving initial rapid burning of part of the trapped gases as shown in Figure 9 where flame speeds of 100 m/s were recorded in the initial part of the trapped gases. This then gave a pressure rise due to the inability to discharge the burnt gases through the vent at this high mass burning rate. This is probably the main reason why the obstacle in the side vented explosions produced the highest overpressures.

CONCLUSIONS

Experimental work was undertaken to evaluate the influence of an obstacle of 40% blockage on side vented explosions and also to directly compare with the end vented explosions. Four pressure peaks were identified and measured due to different stages of the explosion development; the first one (P1) was

due to the initial flame propagation, the second one (P2) was due to the turbulence created by the obstacle, the third one (P3) was due to the external explosion and the fourth one (P4) was due to the pressure oscillations. During side vented explosions and with no-obstacle it was found that the pressure oscillations (P4) was the dominant phase of the explosion whereas during end-vented explosions the explosion was dominated by the external explosion (P3). With the obstacle in place and with side vented explosions the external explosion (P3) to dominated the explosion development. This was in contrast to end vented explosions, where the dominant overpressure was that due to the turbulence created by the obstacle (P2). The maximum overpressure for side vented explosions was much higher compared to end vented explosions and this was mainly due to the turbulence created by the obstacle and further enhanced by the side vent. A turbulent combustion model of the explosion was able to account for the main results with an obstacle, starting from the measured unburnt gas velocities across the obstacle.

ACKNOWLEDGEMENT

We thank the EPSRC for research grant H/40914 in support of this work.

REFERENCES

1. NFPA 68 ,1988, Explosion venting, National Fire Protection Association Inc.
2. Alexiou, A., Andrews, G. E., and Phylaktou, H.,1996, Side - vented gas explosions in a long vessel: The effect of vent position, J. Loss Prev. in Proc. Ind., 9:351-356.
3. Alexiou, A., Andrews, G. E., Gardner, C. L. and Phylaktou H., 1996, The effect of multiple side-venting on gas explosions in large L/D vessels, Trans IChemE, Process Safety and Environmental Protection, Submitted.
4. Rasbash, D. J. and Rogowski, Z. W., 1960, Relief of explosions in duct systems, IChemE Symposium on Chemical Process Hazards, 58-68.
5. Alexiou, A., Phylaktou, H. and Andrews, G. E, 1995, Vented gas explosions with an obstacle, IChemE Symposium Series No. 139: 297.
6. Alexiou, A., Phylaktou, H. and Andrews, G. E., 1996, The effect of vent size on pressure generation in explosions in large L/D vessels, Combust. Sci. Tech., 113-114: 645-652.
7. Phylaktou, H. and Andrews, G. E., 1995, Application of turbulent combustion models to explosion scaling, Trans IChemE, 73 part B:3.
8. Phylaktou, H., Andrews, G. E. Mounter, N. and Khamis, K. M., 1992, Spherical explosions aggravated by obstacles, IChemE Symp. Series ,No 130:525.
9. Phylaktou, H. and Andrews, G. E., 1994, Prediction of the maximum turbulence intensities generated by grid obstacles in explosion-induced flow, 25th Int. Symp. on Combustion, 103.
10. Abdel-Gayed, R. G. and Bradley, D., 1981 A two eddy theory of premixed turbulent flame propagation, Proc. R. Soc. Lond., A 301:1.
11. Phylaktou, H., Andrews, G.E., 1991, The acceleration of flame propagation in a tube by an obstacle, Comb. and Flame, 85:363-379.
12. Engineering Sciences Data, 1978, Flow through a sudden enlargement of area in a duct Item Number 72022 E6 ESDU, London.
13. Engineering Sciences Data, 1973, Pressure losses in three leg pipe junctions, dividing flows, Item Number 73022 ESDU, London.

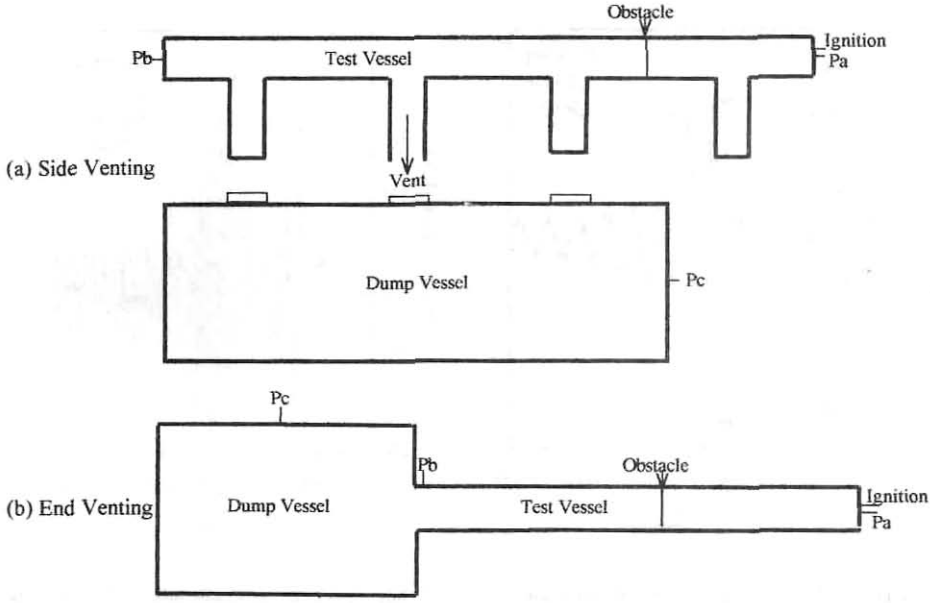

Figure 1. Experimental set up.

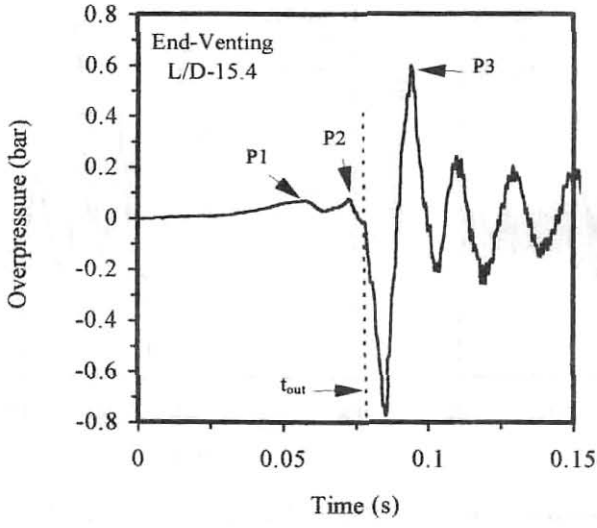

Figure 2. Typical pressure-time history in end vented explosions without obstacle.

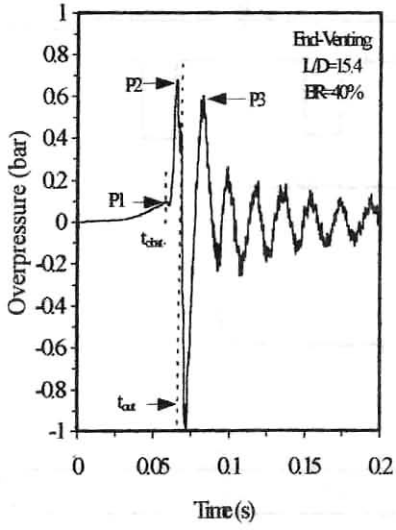

Figure 3. Typical pressure-time history in end vented explosions with an obstacle of BR=40%.

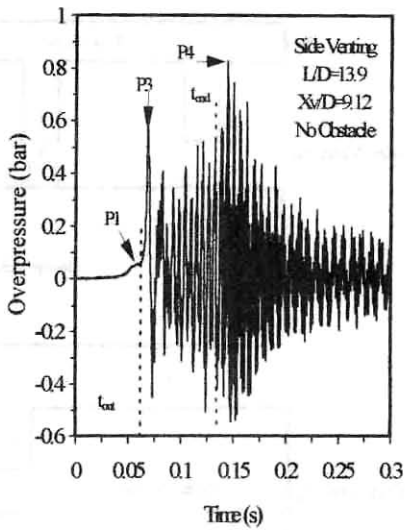

Figure 4. Typical pressure-time history in side vented explosions without obstacle.

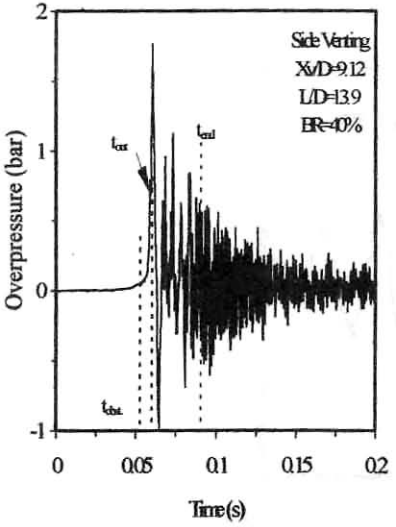

Figure 5. Typical pressure-time history in side vented explosions with an obstacle of BR=40%.

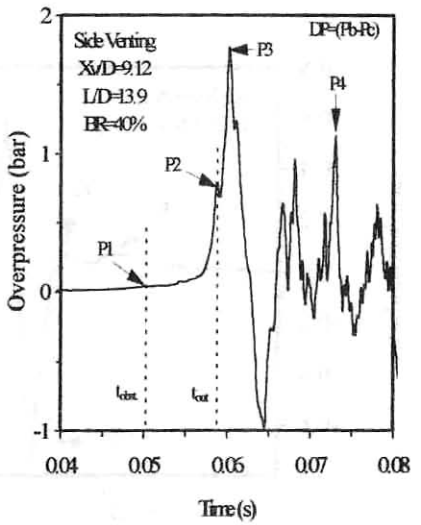

Figure 6. Pressure-time history in side vented explosions taking the difference between the pressure transducers Pb-Pc.

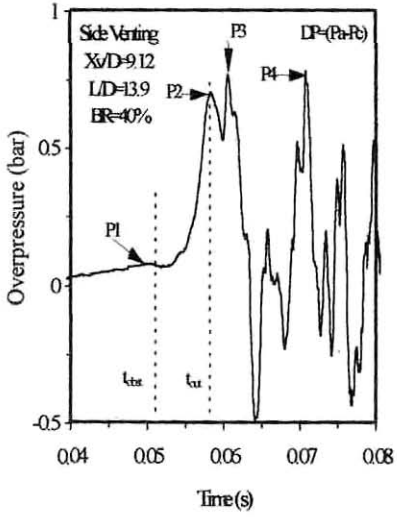

Figure 7. Pressure-time history in side vented explosions taking the difference between the pressure transducers Pa-Pc.

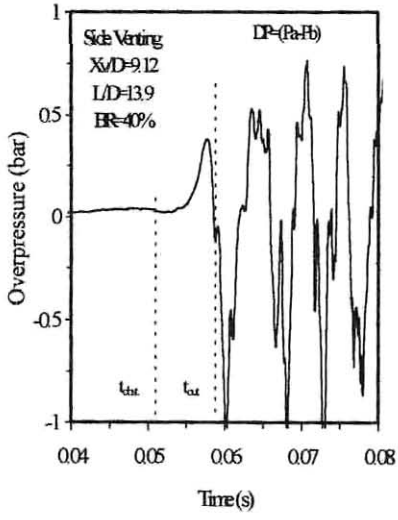

Figure 8. Pressure-time history in side vented explosions taking the difference between the pressure transducers Pa-Pb.

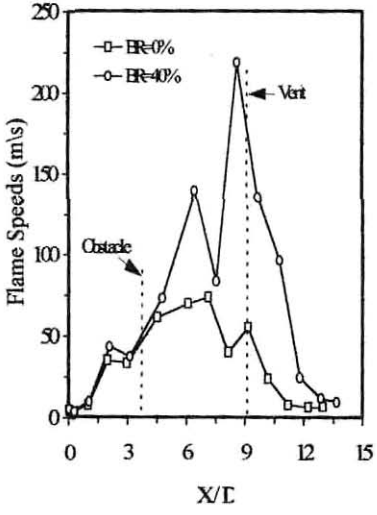

Figure 9. A comparison of flames speeds between obstacle and no obstacle as a function of X/D during side vented explosions.

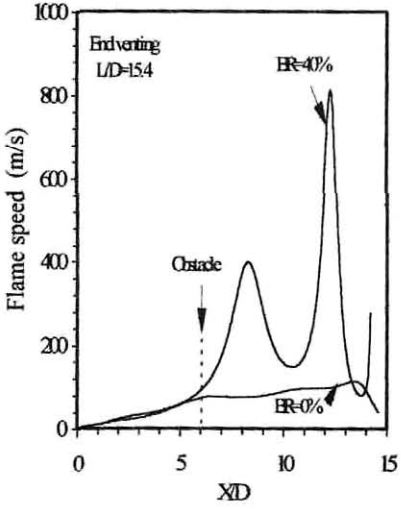

Figure 10. A comparison of flames speeds between obstacle and no obstacle as a function of X/D during end vented explosions.